Effectiveness of Side Force Models for Flow Simulations Downstream of Vortex Generators

Florentie, Liesbeth; van Zuijlen, Alexander; Hulshoff, Steven; Bijl, Hester

DOI
10.2514/1.J055268

Publication date
2017

Document Version
Accepted author manuscript

Published in
AIAA Journal: devoted to aerospace research and development

Citation (APA)
Florentie, L., van Zuijlen, A., Hulshoff, S., & Bijl, H. (2017). Effectiveness of Side Force Models for Flow Simulations Downstream of Vortex Generators. *AIAA Journal: devoted to aerospace research and development*, *55*(4), 1373-1384. Advance online publication. https://doi.org/10.2514/1.J055268

Effectiveness of the BAY model for flow simulations downstream of vortex generators

Liesbeth Florentie *, Alexander H. van Zuijlen†, Steven J. Hulshoff‡
and Hester Bijl§
Delft University of Technology, Delft, The Netherlands

Vortex generators (VGs) are a widely used means of flow control, and predictions of their influence are vital for efficient designs. However, accurate CFD simulations of their effect on the flow field by means of a body fitted mesh are computationally expensive. Therefore the BAY and jBAY models, which represent the effect of VGs on the flow using source terms in the momentum equations, are popular in industry. In this contribution we examine the ability of the BAY and jBAY model to provide accurate flow field results by looking at boundary layer properties close behind VGs. The results are compared with both body fitted mesh and other source term model RANS simulations of 3D incompressible flows, over flat plate and airfoil geometries. We show the influence of mesh resolution and domain of application on the accuracy of the models and investigate the influence of the source term on the generated flow field. Our results demonstrate the grid dependence of the models and indicate the presence of model errors. Furthermore we find that the total applied force has a larger influence on both the intensity and shape of the created vortex than the distribution of the source term over the cells.

I. Introduction

Since their first documentation by Taylor,[1] vortex generators (VGs) have been shown to be able to yield significant performance gains when applied to e.g. airplane wings, wind turbine blades and engine inlet ducts.[2–6] By the introduction of streamwise vortical structures in the boundary layer, VGs effectively mix the high-momentum flow in the outer layer with low-momentum flow close to the surface, thereby re-energizing the boundary layer. This causes the flow to become less susceptible to adverse pressure gradients, such that flow separation can be delayed or even completely overcome. Apart from an increase in aerodynamic lift, and hence for example the achievable power output of a wind turbine, this mitigation of stall can also lower the aero-acoustic noise levels.[6]

VGs are typically small vanes that are mounted on a surface at an angle relative to the incoming flow. Whereas conventional designs have a height larger than the boundary layer thickness, submerged VGs, with a height less than the boundary layer thickness, are becoming more popular due to the smaller drag penalty they impose. In a review by Lin[6] it is shown that submerged VGs can be equally effective in postponing separation, provided that they are positioned close to the original point of separation. It is clear that an optimal effect requires accurate VG design and positioning, therefore detailed simulation tools to study the effect of VGs on the boundary layer are essential.

Engineering codes and lower order modeling tools for the design process have been developed that are able to take into account the effect of VGs to some extent.[7,8] However, detailed CFD simulations remain indispensable. They are necessary to validate and even calibrate the aforementioned engineering models (e.g. by means of airfoil polars including VG effects). Moreover, CFD codes are essential for the study of flow patterns emerging behind new VG designs and their combined effects encountered for VG arrays.

*Ph.D. Candidate, Faculty of Aerospace Engineering, Aerodynamics Group. Kluyverweg 2, 2629 HT Delft, The Netherlands
†Assistant Professor, Faculty of Aerospace Engineering, Aerodynamics Group.
‡Associate Professor, Faculty of Aerospace Engineering, Aerodynamics Group.
§Dean, Faculty of Aerospace Engineering.

However, the large difference in scale between a VG and the surface on which it is applied in general precludes the use of body fitted mesh simulations. Especially when simulating multiple VGs, as required for non-academic test cases, the related computational cost becomes excessive. Moreover, for such geometries grid generation is a non-trivial and time-consuming task. To overcome the latter issue, the use of immersed boundary methods[9,10] and overset (Chimera) grids[2] has been proposed. Although both methods reduce the burden of creating suitable numerical grids for complex VG configurations, they still require mesh refinement around the VGs and therefore still impose a large computational cost.

A more popular and widely used approach therefore consists of modeling the effect the VG has on the flow rather than its detailed geometry. To this end several techniques have been developed, the majority of which are based on the addition of a source term to the governing equations in order to enforce the formation of a vortex with the desired properties. Roughly two groups of such models can be distinguished, those which assume a certain vortex profile a priori, and those which enforce the creation of a vortex without assumptions with respect to the flow profile.

An early example of this first group is the model developed by Kunik,[11] who used governing equations in the stream function-vorticity formulation and added a source term to the vorticity transport equation by assuming a given initial vortex strength and exponential decay rate. Later work by Wendt[12] and May[13] describes models based on an ideal vortex profile enhanced with empirical relations. More recently, Törnblom and Johansson[14] proposed a model for RANS simulations that introduces the cross-stream velocity field associated with the vortices (based on a Lamb-Oseen vortex) indirectly through forcing functions in the Reynolds stress transport equations. This work was later extended by von Stillfried et al.[15] Furthermore, Velte[16] used the assumption of self-similarity and helical symmetry to formulate an alternative VG model, based on the Batchelor vortex model. Although in general being capable of yielding qualitatively and quantitatively good results for specific situations, these models rely on the inherent assumption that the created vortex can be described by an analytic profile, usually in combination with empirical relations. They thus fail to take into account the particular VG geometry and flow characteristics for the situation of interest. This makes these models less suitable for the study of new, unconventional designs.

An alternative to the aforementioned prescribed vortex models is to use source terms in the momentum equation which (approximately) enforce flow tangency on the VG. These trigger the formation of a streamwise vortex, but make no prior assumption on the profile of the final vortex. An example of the latter category is the VG model proposed by Bender et al.[17] (usually referred to as the BAY model), which defines a source term based on the VG orientation and the local velocity in the grid cells corresponding to the VG location. This model, either in its original form or using the modification proposed by Jirasek,[18] is often used in industry. An alternative to the BAY model was proposed by Wallin and Eriksson[19] who used a body force formulation assuming the local forcing to be normal to the VG surface and inversely proportional to the square of the local time scale.

Due to their widespread use in industry, in this work we take a closer look at the BAY and jBAY model. The aim of this study is twofold. On one hand we identify the influence of mesh resolution on the predictive capability of these models with respect to the vortex shape and the boundary layer shape factor. On the other hand, we analyse factors related to the formulation of the source term that influence the accuracy of these models in order to identify possible improvements.

II. The BAY and jBAY models

The BAY model was proposed by Bender et al.[17] in 1999, and since then has been widely implemented in CFD codes.[20,21] The model mimics the effect of VGs on the flow by approximately enforcing flow tangency in a group of cells in the vicinity of the VG location. This is achieved using local source terms in the momentum equation of the form

$$\mathbf{f}_i = cA\frac{V_i}{V_{tot}}\rho\left(\mathbf{u}_i\cdot\mathbf{n}\right)\left(\mathbf{u}_i\times\mathbf{b}\right)\left(\frac{\mathbf{u}_i}{|\mathbf{u}_i|}\cdot\mathbf{t}\right), \tag{1}$$

where A is the VG planform area, V_i/V_{tot} is the ratio of the cell volume to the total volume of cells where the source term is applied, ρ is the fluid density, $\mathbf{u}_i$ the local flow velocity and $\mathbf{n}$, $\mathbf{b}$, and $\mathbf{t}$ are unit vectors defining the direction (respectively normal, spanwise and tangential) of the VG, as indicated in Figure 1. Localized application of the source term formulation (1) results in a source term distribution similar to the force distribution over an airfoil, with the applied forcing being strongest near the location of the leading

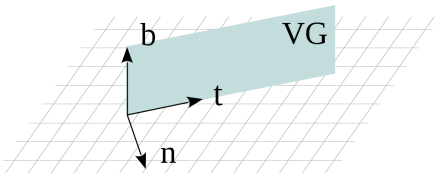

Figure 1. VG orientation vectors.

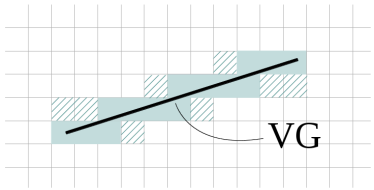

Figure 2. Cells where the source term is applied. Additional cells for the jBAY model are indicated with the striped pattern.

edge of the VG. Note that (1) also contains a constant c which to some extent can be used to calibrate the strength of the source term. For large values of c the model becomes independent of this constant[17,20] and flow tangency to the virtual VG is closely approached. Therefore in general $c > 10$ is advised. In this work, we used $c = 15$ to ensure independence of the results from c.

Originally, Bender et al.[17] proposed defining the region where to apply the source term, hence V_{tot}, by selecting several rows of cells near the VG, the amount of which could be used to calibrate the model. This of course requires the availability of suitable calibration data, and it should be done for every mesh that is used. Due to the inconvenience of this approach, later methods have been proposed that select the cells which overlap the geometry of the VG, and distribute the source term based on the distance between the cell center and a virtual zero-thickness VG plane.[18,22] The jBAY model[18] is the most widely used of these. It calculates the body force using the (interpolated) velocity at the intersections of the VG surface with the grid edges. The resulting local source term is then distributed over the surrounding cells. By enforcing flow tangency at a consistent position, the jBAY model can be expected to have improved accuracy and reduced grid dependence compared to the original BAY model.

In the current work, we use both the original formulation (1) of the BAY model and the jBAY model. The original BAY model is used uncalibrated, applying the source term to those cells which overlap the physical location of the VG (by considering its zero-thickness mean surface), as shown by the colored cells in Figure 2. This is standard practice when no calibration data is available, but implies mesh dependence of the model through the variation of V_{tot} and the position at which deviations in flow tangency are measured. For the jBAY model more cells are normally used to distribute the source term, where we select both the colored and striped cells in Figure 2. The latter are selected such that there is always one cell center positioned at each side of the VG mean surface. This implies that V_{tot} is also mesh dependent in the jBAY approach, but the position at which deviations in flow tangency are measured remains fixed.

III. Description of study

III.A. Objective and approach

In this study we examine the error introduced to a Reynolds averaged Navier Stokes (RANS) simulation when using a source term model for computing wall bounded flows over VGs. The errors in flow properties immediately downstream of the VG are obtained by comparison with results from well refined body fitted mesh simulations. The evolution further downstream is not considered as it is governed by the interaction between the initial vortex and the turbulence model, and is thus dependent on the choice of turbulence model rather than the VG model.

An overview of the errors related to different simulation approaches during vortex evolution is contained in Figure 3. Firstly an error in the boundary layer development, and therefore in the initial condition for the vortex development process, is introduced by the choice of using RANS instead of DNS. Furthermore, the use of a VG model instead of a body fitted mesh for the VG adds an error related to the vortex formation. This is usually combined with a discretization error due to the use of an underresolved mesh. Another error source consists of the subsequent interaction between the created vortex and the turbulence model. In this work we only focus on errors related to the VG model. Errors related to the choice of turbulence model are outside of the scope of this study.

To isolate the effect of replacing a geometrical feature with a source term in the governing equations (the VG model error), we study the flow profile during the vortex formation and early propagation phase when there is still some separation between the vortex and the turbulence length scales.[23] Fine mesh results

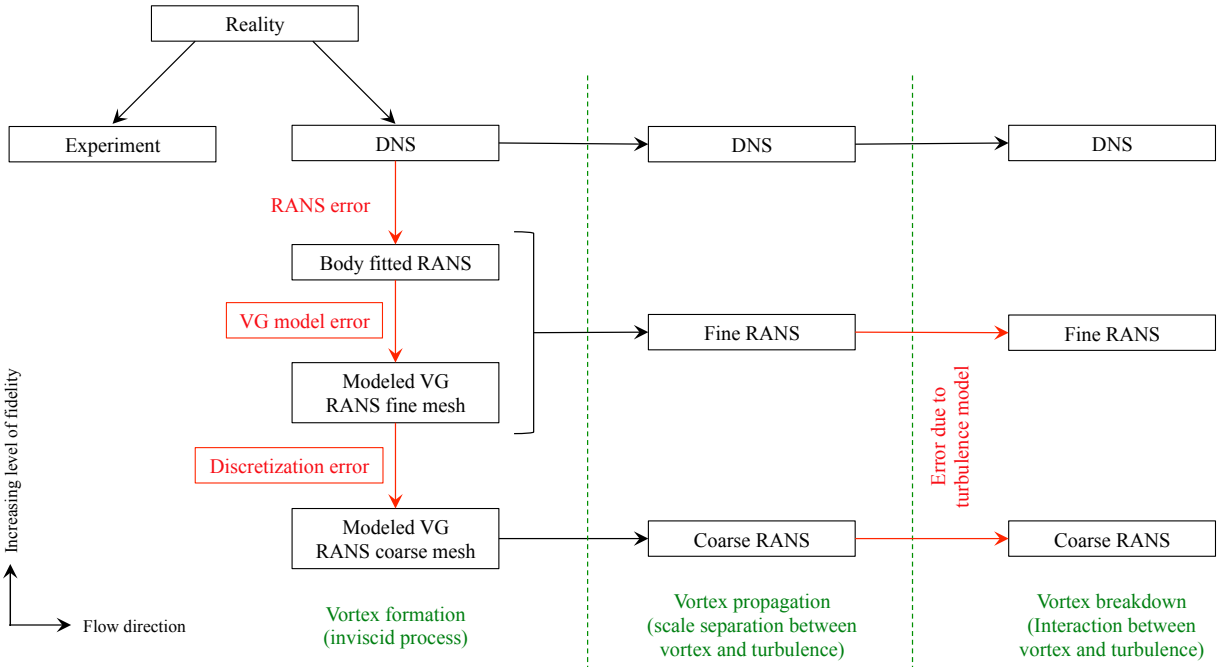

Figure 3. Overview of error sources (in red) related to the RANS simulation of wall bounded flows over VGs. Black arrows indicate a theoretical lack of error.

obtained with the BAY model and variations to the BAY model are compared against body fitted mesh simulations, while using the same numerical settings and similar grid resolution. This way sources of error between both simulation types, other than the VG model error, are effectively minimized. An extra validation with experimental data is included in order to ensure that the numerical results are in line with the physical flow field. Due to the presence of RANS turbulence model errors this data is, however, not used to study the errors related to the VG model.

In the analysis of the BAY model it is observed that errors of the model can originate from two sources. Firstly from the selection of cells where the source term is applied (i.e. the geometry defining V_{tot}), and from the formulation used to compute the source term. The effect of the latter can be investigated by comparison of the BAY model with a source term consisting of the exact VG surface forcing, see section III.B. Furthermore, practical use of the BAY model is generally done in combination with a low resolution mesh, thus also introducing a discretization error. The effect of mesh resolution on the accuracy of the BAY model, and the improvement of the jBAY model in this respect, is considered here by studying the change in results obtained for different mesh refinement levels in the neighborhood of the VG.

This study focuses for a large extent on the qualitative comparison of the flow topology close behind the VG. Research by Spalart et al.[23] has indicated that RANS errors are not dominant until a vortex starts aging. Although no boundary is quantified for this region, based on e.g. the results in Figure 6 we believe that up to $15h$ downstream of the VG trailing edge weak interaction between the vortex core and the largest turbulent length scales can be assumed. Flow field snap shots and shape factor (H) profiles are therefore studied in this region. The shape factor serves as an important indicator for the boundary layers susceptibility to separation and is defined as the ratio between the boundary layer displacement and momentum thicknesses, which for incompressible flow equals

$$H = \frac{\delta^*}{\theta} = \frac{\int_0^\infty \left(1 - \frac{u(z)}{u_\infty}\right) \mathrm{d}z}{\int_0^\infty \frac{u(z)}{u_\infty}\left(1 - \frac{u(z)}{u_\infty}\right) \mathrm{d}z}, \tag{2}$$

where z is the wall normal direction and u_∞ is the freestream velocity. Low values for H indicate an attached boundary layer, whereas in general for $H > 4$ the flow is separated from the surface. Improving the shape factor profiles during vortex development is believed to enhance the overall separation prediction accuracy of the VG model. However, results concerning separation locations are not considered here, since these would include RANS turbulence model errors, thereby making statements about the VG model error ambiguous.

Despite the focus on the flow topology close behind the VG, also a look is taken at the downstream vortex development. To this end the peak streamwise vorticity in the vortex core (ω_{max}), circulation ($|\Gamma|$), decay ($|\Gamma|/|\Gamma_{ref}|$) and the vortex core radius (R) are considered. The latter is calculated as the radius of an equivalent circular vortex, $R = \sqrt{A/\pi}$, considering only the vortex area A where the streamwise vorticity $\omega > 0.1 \cdot \omega_{max}$. Circulation is defined in this work as the integral of only the positive streamwise vorticity, thus excluding the layer of negative vorticity occurring close to the wall in these flows.

III.B. Numerical set up

The numerical results presented in this work are obtained with the open source CFD package OpenFOAM, which is a segregated finite volume code able to solve both compressible and incompressible flows using either structured or unstructured grids.

For the considered VG cases, the steady, incompressible RANS equations are solved using the SIMPLE algorithm, and the governing equations are solved on structured hexahedral grids using first order (the flat plate case) or second order (the airfoil case) upwind discretization schemes for the convective terms. The linear systems arising from the equation discretization are solved using the preconditioned (bi-) conjugate gradient method with diagonal incomplete Cholesky and LU preconditioners for the symmetric and asymmetric systems respectively. Closure of the RANS equations is provided by Menters $k-\omega$ SST turbulence model,[24] ensuring dense near wall meshes with $y^+ < 1$ to allow the viscous sublayer to be resolved.

Six different approaches are considered to include VGs in the simulations:

- **Body fitted mesh**: the flow around the actual VG geometry is resolved by making use of body fitted meshes. In the current work, this is considered to yield the best result achievable within the limitations of the selected numerical framework.
- Flow tangency models:
  - **BAY model:** The original BAY model as discussed in section II.
  - **jBAY model:** Adaptation of the BAY model according to Jirasek,[18] discussed in section II.
- Total force models: These are introduced here to help isolate the main factors contributing to the errors in the flow tangency models, by identifying the effects of the distribution of the source term and the total force that is added to the simulation.
  - **Uniform BAY model**: A uniformly distributed source term is locally added to the momentum equation such that the source term per unit volume is constant over the selected cells and the total applied force equals the total force added to the flow by the BAY model. Hence, in the selected cells a source term

$$\mathbf{f}_i^{UB} = \frac{V_i}{V_{tot}}\mathbf{F} \qquad \text{with} \qquad \mathbf{F} = \sum_{i=1}^{N} \mathbf{f}_i \tag{3}$$

    is applied, where N equals the number of cells where this source term is added. Compared to the BAY model this implies that the applied source term is no longer focused near the leading edge of the VG.
  - **Uniform exact source term** (uniform $\mathbf{F}_{exact}$): Similar to the uniform BAY model, a uniformly distributed source term is added to the momentum equation in the cells selected to correspond with the VG location. In this case, however, the magnitude and direction of the resultant applied force correspond exactly with the total surface force acting on the VG in a body fitted mesh simulation. Hence, the applied source term equals

$$\mathbf{f}_i^{UE} = \frac{V_i}{V_{tot}}\mathbf{F}_{exact} \qquad \text{with} \qquad \mathbf{F}_{exact} = \oiint_{S_{VG}} \tilde{p}\,\mathbf{n}\,\mathrm{d}S, \tag{4}$$

    where S_{VG} represents the surface of the VG, $\tilde{p}$ is the stress (pressure and viscous) acting on the VG surface for a body fitted mesh VG simulation and $\mathbf{n}$ indicates the wall normal direction.

– **Distributed exact source term** ($\mathbf{F}_{exact}$): In this case we do not only calibrate the total force added to the system, but also the distribution of the source term over the cells is matched as close as possible with the actual VG surface force distribution. This is achieved by first calculating the VG force in every interior VG cell of the body fitted mesh by integration over its faces as

$$\tilde{\mathbf{f}}_i^E = \oiint_{S_i} \tilde{p}_i \mathbf{n}_i \, \mathrm{d}S. \tag{5}$$

Afterwards this force distribution is mapped onto the uniform grid and calibrated to account for interpolation errors as

$$\mathbf{f}_i^E = \left(\tilde{\mathbf{f}}_i^E\right)_{bf \mapsto uni} \frac{\mathbf{F}_{exact}}{\sum_i^N \left(\tilde{\mathbf{f}}_i^E\right)_{bf \mapsto uni}}. \tag{6}$$

This distributed $\mathbf{F}_{exact}$ approach theoretically represents the highest accuracy that could be reached with a BAY-like model, as it replaces the VG geometry with exactly the force it imposes on the flow. Hence, the error related to the BAY model due to the approximation of the VG force is eliminated.

In the following, the considered VG models are used on a structured mesh with the same wall normal resolution as the body fitted VG simulations, but with uniform mesh spacings in streamwise and cross-flow directions. The influence of mesh resolution is demonstrated considering refinements in streamwise and cross-flow direction only. For the body fitted mesh simulations grid independence is shown using mesh refinements in all three directions.

III.C. Test cases

The analysis is performed for two test cases simulating (rectangular) vane-type counterrotating VGs. First a zero pressure gradient (ZPG) flow over a flat plate is considered, after which the findings are verified for an airfoil section.

III.C.1. Flat plate

The flow over a flat plate with an array of counterrotating, common down, vane-type rectangular VG pairs is considered, in accordance to the experimental set up reported by Baldacchino.[25] The experimental data is obtained for submerged VGs with a height of approximately $h = \delta/3$. An overview of the numerical parameters is included in Table 1.

The numerical simulations are performed for one VG pair only, using symmetry boundary conditions in order to account for the effect of neighboring VG pairs. The inflow boundary is located 5 boundary layer heights before the leading edges of the VGs. A fully turbulent inflow profile is specified such as to yield a boundary layer thickness of $\delta = 15\,\mathrm{mm}$ at the trailing edges of the VGs.

For both the body fitted mesh and the uniform mesh a small wall normal mesh spacing is used, ensuring $y^+ < 1$ for both the flat plate and the VG surfaces. In the streamwise and cross-flow directions different

Table 1. Test case parameters as defined in Figure 4

Parameter	Symbol	Value	
		Flat Plate	Airfoil
Configuration	-	common down	common up
Freestream velocity	U_∞	15 m/s	24 m/s
Boundary layer thickness	δ	15 mm	6 mm
VG height	h	$\delta/3$	δ
VG length	l	$2.5h$	$3h$
Inflow angle	β	18 °	20 °
VG TE distance	d	$2.5h$	$3.7h$
Pair distance	D	$6h$	$11.7h$

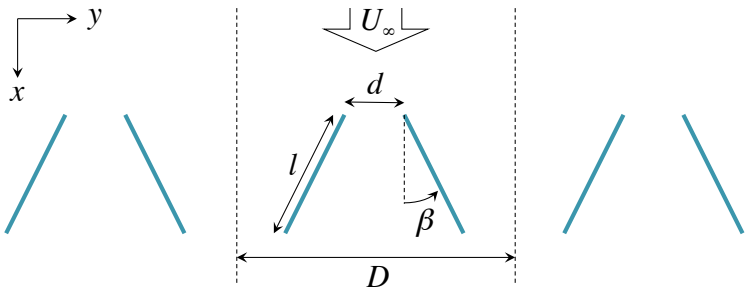

Figure 4. Illustration of a common down VG array layout and the corresponding parameters. The dotted line indicates one VG pair, as included in the simulation of the flat plate test case.

cell sizes have been used, varying from $N_s = 32$ cells in cross-flow direction per VG pair (corresponding to $\Delta \approx 0.2h$) for the coarsest uniform mesh to $N_s = 176$ for the body fitted mesh (see Table 2). The mesh spacing for the body fitted mesh is verified to be dense enough to yield a grid independent solution, as shown in Figures 6 and 8. The estimate for the discretization error related to the shape factor H is found to be $\epsilon \approx 0.3\%$ for the finest mesh.

III.C.2. Airfoil

In order to verify our findings for a more industrial relevant application, a 3D airfoil section is considered. The chosen airfoil profile has a thickness-to-chord ratio of 18% and is designed for use on variable pitch and variable speed multi MW wind turbines. The effect of delta shaped VGs for this airfoil has been studied experimentally by Manolesos et al.[26] for a Reynolds number of 0.87×10^6.

The set up used in this work is based on the configuration of Manolesos,[26] however, using rectangular VGs instead of delta VGs. This is done in order to enhance the similarity with the flat plate case and to facilitate a straightforward construction of a quality body fitted mesh. For the current analysis we used an angle of attack of $\alpha = 10^\circ$ and we included counterrotating common up VG pairs at 30% of the chord. This corresponds to a distance of approximately 21 VG heights before the point where boundary layer separation would occur in absence of VGs. More details with respect to the VG set up are included in Table 1.

Body fitted mesh and source term simulations are performed for a slice of the domain containing half a VG pair, using again symmetry boundary conditions to account for the neighboring VGs. An O-grid mesh is used with the farfield boundary located 50 chord lengths away from the airfoils leading edge and ensuring $y^+ < 1$ on the airfoil and VG surfaces. Mesh convergence is shown for the body fitted mesh simulations in Figures 6 and 8, yielding an error estimate of $\epsilon \approx 0.6\%$ for the shape factor profiles.

For the source term models, the mesh is locally refined in the neighborhood of the VG, with the number of cells in cross-flow direction varying from $N_s = 18$ to $N_s = 72$, as indicated in Table 2. Although the computational resources employed for the airfoil case were larger than those used for the flat plate, the relative mesh resolution was less due to the extent and complexity of the domain. The resolutions used for the airfoil case are, however, similar to those used in an applied setting.[27]

Table 2. Mesh details for the flat plate and airfoil test cases, with N the total number of cells, and N_s the number of cells in cross-flow direction for one VG pair (the distance D).

		Body Fitted			Uniform		
		coarse	medium	fine	coarse	medium	fine
Flat Plate	N	0.4×10^6	1.6×10^6	6.4×10^6	0.3×10^6	1.2×10^6	4.6×10^6
	N_s	44	88	176	32	64	128
Airfoil	N	0.3×10^6	2.2×10^6	17.8×10^6	2.0×10^6	4.3×10^6	9.9×10^6
	N_s	32	64	128	18	36	72

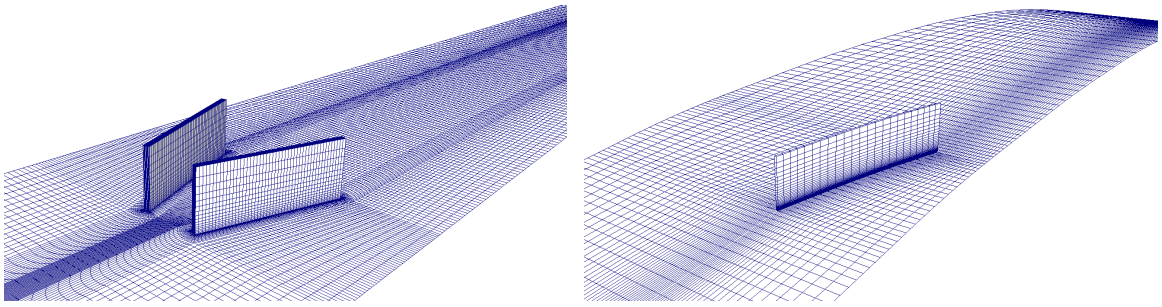

(a) Flat plate (b) Airfoil

Figure 5. Detail of the body fitted meshes with medium grid resolution.

IV. Influence of mesh resolution on the performance of the BAY and jBAY models

Numerical simulations of the flat plate and airfoil test cases are performed using several mesh resolutions in order to identify the effect of grid refinement on the flow field obtained with the BAY and jBAY model. Starting from a coarse grid, medium and fine grids are constructed by refining by a factor 2 in streamwise (x) and cross-flow (y) directions. In this section we will first study the BAY model and afterwards discuss its differences with the jBAY model. Results regarding the downstream evolution of the created vortex in terms of peak vorticity, circulation, decay and core radius closely downstream of the VG, are shown in Figures 6 and 7. Furthermore the shape of the boundary layer disturbance is studied by considering shape factor profiles close behind the VG (Figure 8). These figures also contain body fitted mesh results on different grids in order to demonstrate the grid independence of the validation data. Moreover, some experimental data points for peak vorticity, circulation and decay are included for the flat plate case, which show good agreement with the body fitted mesh results. Note that the obtained absolute circulation values are larger than the experimental data points, which is partly due to differences in the definition of the vortex core region.

From Figures 6(a), 6(d) and 7(a) a large dependence on grid resolution of the vortex core peak vorticity and the vortex core radius is observed. The latter is related to the variations with grid resolution of the peak vorticity due to its definition being based on this quantity. Peak vorticity is observed to increase with increasing mesh refinement, due to the vortex becoming more concentrated. Especially for the airfoil case the variation in results is large, due to the discretization error being more pronounced for the affordable levels of resolution used. In Figures 6(a), 6(b), 7(a) and 7(b) also the typical underestimation of the vortex intensity when using the BAY model can be observed. This drawback of the BAY model was already identified in previous publications.[23,28] Despite the grid dependence of peak vorticity, this underestimation is considered to be a property inherently related to the BAY model. The use of grid densities beyond the finest uniform mesh used in this work would increase the computational cost significantly, thereby largely reducing the advantage of using a source term model. It should be noted though, that for cases with high fidelity data available this issue might be alleviated by tuning the model by means of selecting more cells,[17] thereby changing the volume V_{tot} where the forcing is applied. This will be further elaborated upon later in this section.

The circulation and, especially, the decay of the created vortex (Figures 6(b), 6(c) and 7(b)) prove to be less grid dependent than the peak vorticity, as expected due to those being integral quantities and therefore being less prone to local high frequency errors. This allows one to obtain a nice view on how the BAY model performs in this respect. From the circulation decay results it follows that a model error seems to be present. The initial vortex decay due to the cancellation of primary vorticity with opposite vorticity that is lifted from the wall seems not to be captured well. The BAY model therefore yields a vortex which initially decays slower than when using a body fitted mesh. Further downstream, when the interaction between the vortex and the turbulence model starts to dominate the decay, the decay rate is similar to the body fitted mesh result. It is observed that this difference in initial decay rate to some extent cancels the underestimation of the vortex circulation further downstream.

A closer look at the boundary layer profile confirms the presence of a model error. The shape factor profiles, shown in Figure 8 for both the flat plate and the airfoil cases, are initially very different from

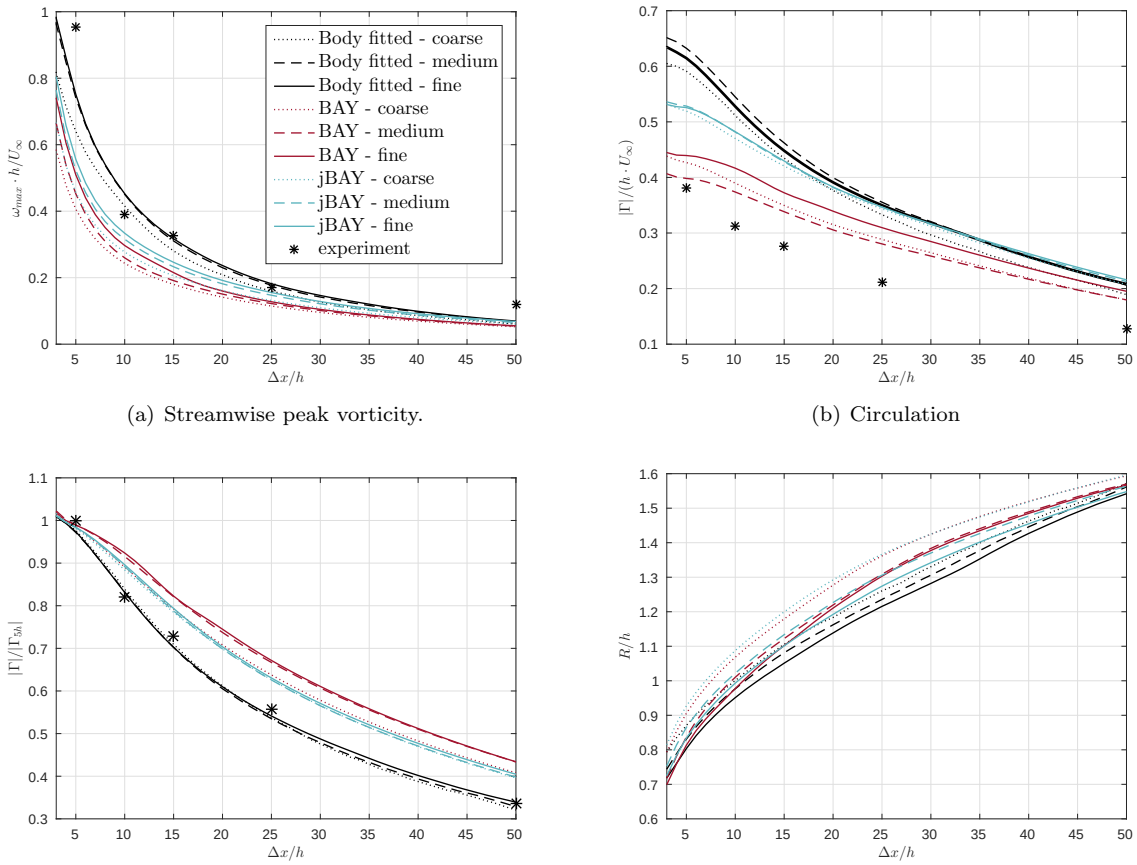

(a) Streamwise peak vorticity.

(b) Circulation

(c) Circulation decay.

(d) Core radius for an equivalent circular vortex.

Figure 6. Vortex evolution downstream of the VG pair on the flat plate for different mesh resolutions for the body fitted mesh and the BAY and jBAY models.

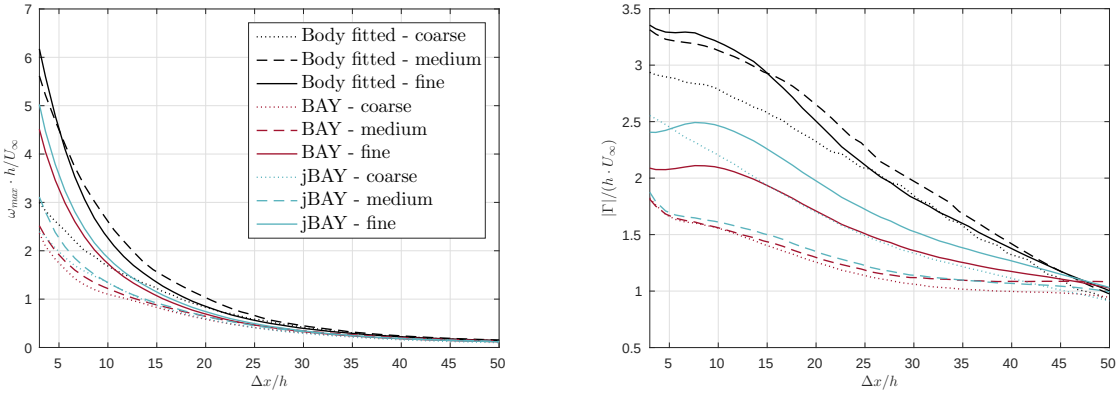

(a) Streamwise peak vorticity.

(b) Circulation

Figure 7. Vortex evolution downstream of the VG on the airfoil for different mesh resolutions for the body fitted mesh and the BAY and jBAY models.

the body fitted mesh result. The peaks have different values and are at different locations. This indicates a difference in boundary layer disturbance, rather than an underestimation of the vortex intensity only. These differences in the boundary layer profile propagate downstream, and are therefore likely to influence predictions related to the effect of the VGs. However, as the vortex dissipates the shape function error decreases. Further research is therefore required to quantify the effect of this error on the prediction of

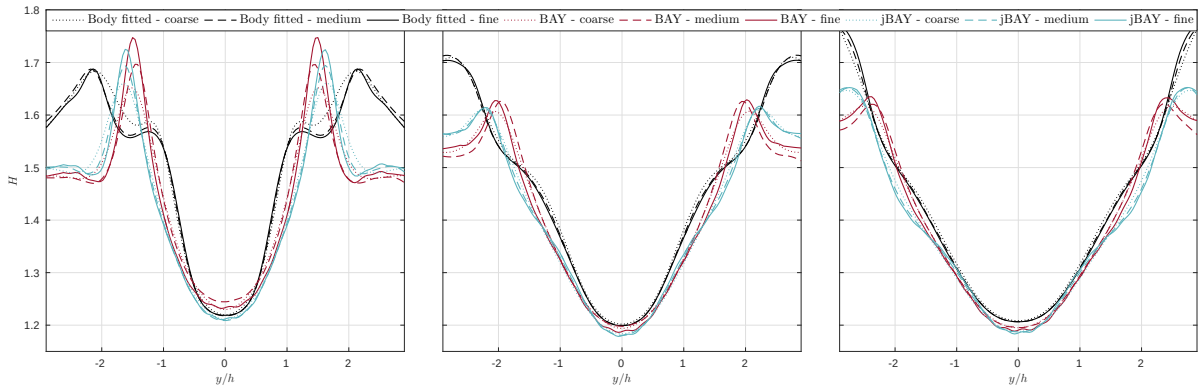

(a) Flat plate with submerged common down VG pair ($h \approx \delta/3$).

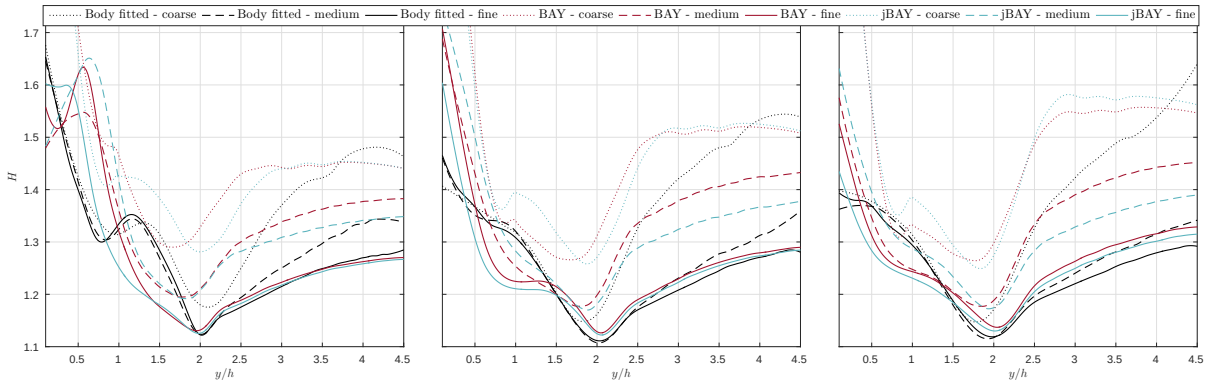

(b) Airfoil section with common up VG pair ($h \approx \delta$).

Figure 8. Effect of mesh resolution on the shape factor for the BAY and jBAY models, at (from left to right) $\Delta x = 5h$, $\Delta x = 10h$ and $\Delta x = 15h$ behind the VG pair.

boundary layer separation.

When looking at the shape factor variations upon grid refinement, we see that initially the result is largely dependent on mesh resolution. This is mainly clear from the airfoil shape factor results, using the BAY model in combination with rather coarse meshes. Hence a certain minimum grid resolution is required in order to obtain meaningful results with the BAY model. For the flat plate case higher grid resolutions are used, resulting in only small differences in the shape factor profiles. This indicates that beyond a certain level of grid resolution the flow profile does not significantly change anymore upon grid refinement.

As mentioned before, this grid dependency of the BAY model can be explained by the selection of the cells where the model is applied. Upon mesh refinement the forcing is applied in an increasingly confined region. This implies (i) that flow tangency is enforced closer to the actual VG location, (ii) that the distribution of the applied source term becomes smoother, but also (iii) that the total volume V_{tot} where the source term is applied decreases. The first two of these consequences are similar to standard discretization errors and can be expected to decrease upon mesh refinement. However, when selecting cells based on the VG mean surface (as done in this work), V_{tot} will keep on decreasing with mesh refinement. Therefore solutions obtained with the BAY model will not become completely grid independent.

The jBAY model[18] was proposed in order to improve accuracy and reduce mesh dependency of the original BAY model. Indeed, our results indicate that the jBAY model produces a stronger vortex, yielding a smaller error with respect to peak vorticity (Figure 6(a)) and increased flow circulation (Figure 6(b)). Apart from the intensity, however, the boundary layer disturbance is very similar as for the BAY model, as can be seen from the much alike shape factor profiles. Furthermore, the grid dependency indeed seems to be reduced. When looking at the circulation and decay (Figures 6(b) and 6(c)) a seemingly grid independent solution is reached for the coarse mesh already, whereas for the BAY model this is only the case for circulation decay

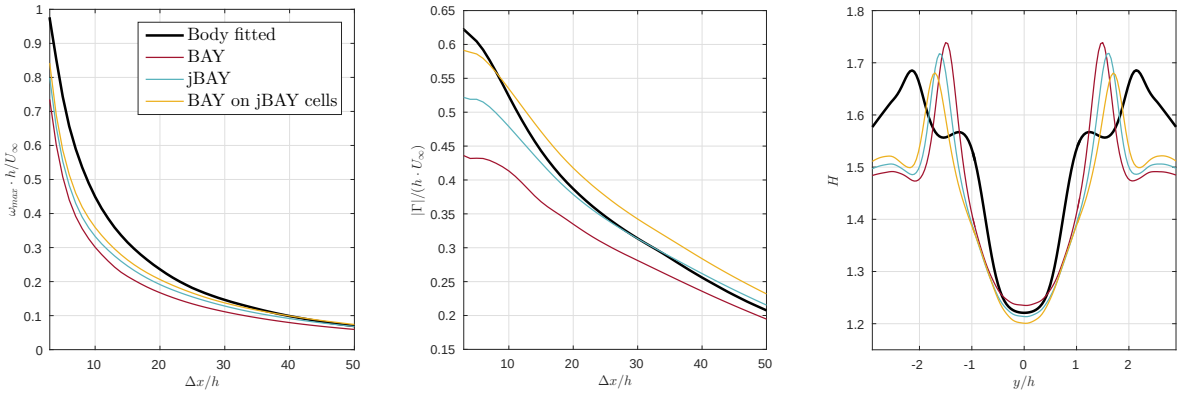

(a) Streamwise peak vorticity. (b) Circulation. (c) Shape factor at $\Delta x = 5h$.

Figure 9. Fine mesh results to illustrate the effect of V_{tot}.

on the medium grid. Also the flat plate shape factor profiles on the medium and the fine mesh differ less than for the standard BAY model. This is attributed to the improved formulation of the model yielding flow tangency to be imposed at a consistent location, thereby eliminating this source of grid dependence from the BAY model. Moreover, the distribution of this forcing over two cells in cross-flow (y) direction instead of only one allows for a smoother application of the forcing to the flow field. Both factors cause the jBAY model to exhibit a reduced grid dependence compared to the BAY model. However, also this model keeps a dependency on grid resolution due to the volume V_{tot} where the source term is applied, which reduces upon mesh refinement and thereby decreases the size of the created vortex.

To take a closer look at this impact of V_{tot} an additional simulation was performed, in which the BAY model was applied using the same cells as for the jBAY model, so using both the solid and striped cells in Figure 2. Results were obtained for the flat plate case on the finest mesh to minimize the effect of discretization errors, and are included in Figure 9. Here V_{tot} of this additional simulation is equal to V_{tot} of the jBAY model simulation and approximately 63% larger than for the conventional BAY model simulation. The results show that increasing V_{tot} by the addition of cells where the BAY model is applied has a large effect on the strength of the created vortex. Both the total circulation and the peak vorticity in the vortex core are clearly increased (Figures 2(a) and 2(b)). Moreover, a wider part of the boundary layer is disturbed, as seen from the shape factor profile in Figure 2(c). In Table 3 the total forcing $|\mathbf{F}_{tot}|$ (the integrated source term) is included. Whereas this force is little influenced by mesh refinement, the addition of extra cells yields a significant increase in $|\mathbf{F}_{tot}|$.

These observations suggest that a certain total force is required to align the flow in a specific region of the domain with the VG direction. Furthermore, this total force seems to be directly related to the created circulation in the flow. The addition of cells where the BAY model is applied effectively increases the region where the flow direction should be altered, and therefore more forcing is thus added to the flow by the BAY model in order to obtain sufficient circulation to achieve this. Due to the resulting increase in circulation, the peak vorticity also rises. Moreover, because the source term is now distributed over a wider region a larger part of the boundary layer is disturbed, such that a vortex with a larger radius is created.

Compared to the BAY model, the jBAY model aims to align the flow with the VG direction in a smaller region due to the location where flow tangency is evaluated. A smaller force and less circulation is thus required to achieve this change in flow direction. Moreover, the interpolation and redistribution procedures of the jBAY model cause the applied source term to be more concentrated towards the actual VG location. This results in a slightly smaller region of the boundary layer being disturbed.

Overall, we find that both the BAY and the jBAY model (initially) underpredict the vortex strength and create erroneous shape factor profiles, when compared with body fitted mesh simulations. The jBAY model yields an improved solution over the BAY model in the sense of reduced grid dependency and the creation of a stronger vortex. It might be possible to tune the value of circulation provided by the BAY model by adding cells to which the model is applied, but this does not seem to improve the representation of the shape factor downstream of the VG. Moreover, it reduces the accuracy of the flow representation in the neighborhood of the VG due to the alignment of the flow in a larger region.

Table 3. Components of the total VG force, the VG volume and the resultant VG force per unit volume. All quantities are normalized by the body fitted mesh (BF) result and obtained on the finest mesh, unless specified otherwise.

Case	Model	$\mathbf{F}_n$	$\mathbf{F}_t$	$\mathbf{F}_b$	$\lvert\mathbf{F}_{tot}\rvert$	V_{tot}	$\lvert\mathbf{f}\rvert$
Flat plate	BAY (coarse)	0.769	0.075	0	0.773	2.706	0.287
	BAY	0.735	0.073	0	0.739	0.634	1.169
	BAY (jBAY cells)	0.957	0.079	0	0.961	1.036	0.931
	jBAY	0.859	0.078	0	0.863	1.036	0.836
	BF	0.973	0.217	0.084	1	1	1
	BF (inviscid)	0.973	0.192	0.073	0.994	1	0.994
Airfoil	BAY (coarse)	-0.674	-0.044	0.013	0.675	11.125	0.061
	BAY	-0.654	-0.036	0.014	0.655	2.284	0.287
	jBAY	-0.740	-0.050	0.015	0.742	3.842	0.193
	BF	-0.995	0.021	0.099	1	1	1
	BF (inviscid)	-0.993	0.002	0.082	0.997	1	0.997

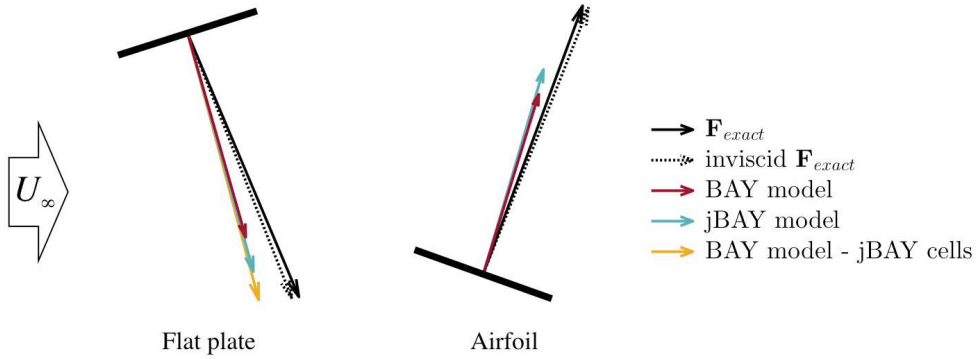

Figure 10. Visualization of the resultant VG force in the x-y plane.

V. Effect of magnitude and distribution of the source term

In the previous section it was observed that there is a deviation between the flow profile obtained with the BAY model and with body fitted mesh simulations, which cannot be alleviated by mesh refinement or the addition of cells, and which is not resolved by the jBAY model. In this section we therefore investigate different source term properties with respect to their potential in altering the obtained flow field. For this purpose, the total force added to the flow by the source term, and the distribution of this source term over the selected cells, are studied. This is done by considering the total force models "uniform BAY", "uniform $\mathbf{F}_{exact}$" and (distributed) "$\mathbf{F}_{exact}$", as introduced in section III.B. To minimize the discretization error all data is obtained on the fine meshes.

First the total VG force as approximated by the BAY model is compared to the actual VG surface force obtained from the body fitted mesh simulations in Table 3. Apart from the components of the resultant force in normal, tangential and VG spanwise direction, this table also contains the total resultant force $|\mathbf{F}_{tot}|$ and the forcing per unit volume $|\mathbf{f}|$. All data in Table 3 is normalized by the body fitted (BF) mesh result, and V_{tot} indicates the volume of the VG (body fitted mesh) or the selected cells (source term models). Moreover, the resultant forces in the $x-y$ plane are visualized in Figure 10. It follows that for both considered cases the BAY model underpredicts the force acting on the flow varying from 26% to 34% (which reduces to 14% to 26% for the jBAY model). Furthermore, an error in orientation of 7 degrees is observed, which seems to be mainly due to the large error in the tangential VG force. Comparison with the inviscid VG force (inv. BF), so considering only the pressure force acting on the VG surface, illustrates that this deficit is much larger than what can be attributed to the absence of the wall shear stress contribution in the BAY model.

A closer look at the force components reveals that whereas all components are underestimated, the largest

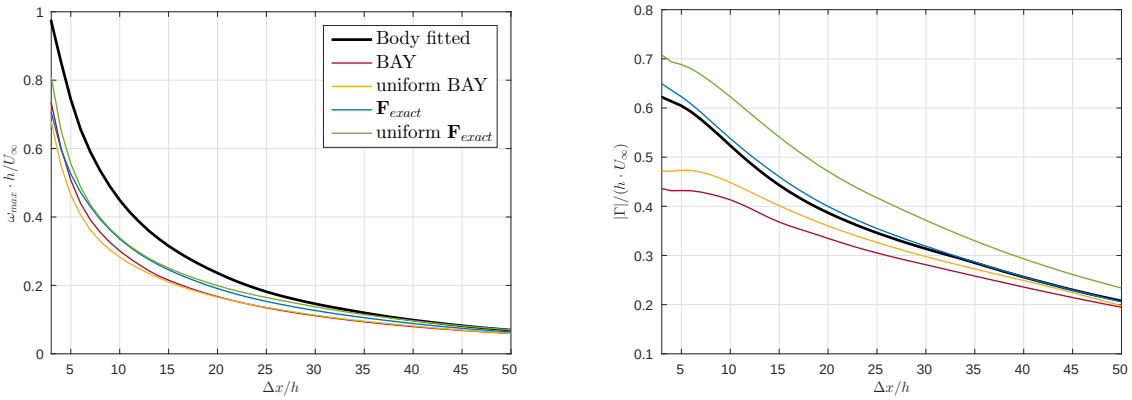

(a) Streamwise peak vorticity.

(b) Circulation.

Figure 11. Vortex evolution downstream of a VG pair on a flat plate for different source term variations.

relative deviation is in the components parallel to the VG surface (i.e. in the direction of **t** and **b**). This can be partly explained by the large relative contribution of viscosity, which is neglected in the BAY model. The component along the span of the VG is even absent for the flat plate case. This suggests an inability of the BAY model to adequately deal with cross flow and roll up over the top edge of the VG, both of which are important flow patterns when considering low aspect ratio geometries like typical VGs. Despite their small magnitude, these secondary components (especially $\mathbf{F}_b$, in spanwise VG direction) directly contribute to the swirling motion of the flow. Their non-negligible influence on the generated flow field is visible in Figures 12 and 13, showing streamwise velocity and vorticity snap shots up to $15h$ behind the VG. Visual comparison with experimental data confirms that the body fitted mesh results correspond to the physical flow field. When looking at the source term model simulations, it is observed that the $\mathbf{F}_{exact}$ source term (results (e)) yields a strong improvement in capturing the uplifting of fluid from the wall, resulting in a vortex shape that is more similar to the body fitted mesh result than the BAY model (results (c)). This effect, which is also visible in the shape factor profiles (Figure 14) by the improved peak locations, is believed to be directly attributable to the force component in VG spanwise direction $\mathbf{F}_b$.

Moreover, the distribution of the source term over the selected cells seems to have a smaller effect on the created vortex (both in terms of intensity and shape) than does the magnitude and direction of the total force added by the source term. A uniformly distributed source term with the exact total force components (uniform $\mathbf{F}_{exact}$) is able to yield an improved representation of the flow field compared to the BAY model. This effect becomes also clear when comparing the deviation between the results for the BAY model and the uniform BAY model (results (c) and (d)) to the deviation between the uniform BAY model and the uniform $\mathbf{F}_{exact}$ model (results (f)). The latter difference seems to be more pronounced.

Furthermore, when considering the overall vortex evolution a large improvement is possible when the total force is closer to the actual VG force. This is visible in Figure 11, and was also already observed in Figure 6 for the jBAY model. Apart from the direct and intuitive effect on the vortex intensity, a positive effect on the initial circulation decay is observed. This is attributed to the improved representation of the uplifting of the layer with negative vorticity close to the wall. In the case of the flat plate flow, this initial flow field improvement for the $\mathbf{F}_{exact}$ model even yields a nearly perfect representation of the circulation and decay further downstream as well.

Opposite to the jBAY model formulation, which does not yield a change in shape factor profile, adaptation of the total force added to the flow is observed to do so. However, it should be noted that although improving the added total force seems to be very beneficial, it does not entirely resolve the deviation in shape factor profile close behind the VG. This is shown in Figure 14, which indicates a large spread in the results for the different methods. Even the $\mathbf{F}_{exact}$ model does not succeed in yielding a perfect match to the body fitted mesh results. These remaining deviations may be expected to have an impact on the prediction of the overall VG effect (e.g. with respect to flow separation), as initial errors in the boundary layer profile propagate downstream. Further research should be performed to determine how the ability of different turbulence models in predicting separation are affected by the velocity field introduced by vortex generators.

The above observations with respect to the resultant source term force and the source term distribution

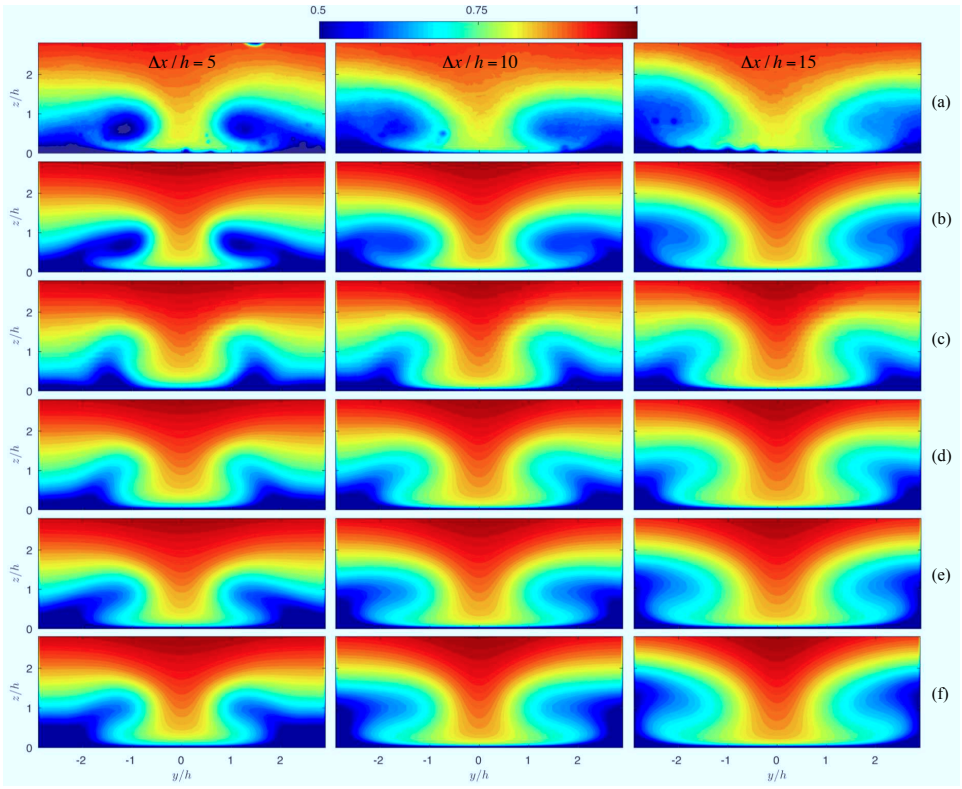

(a) Streamwise velocity (U_x/U_∞)

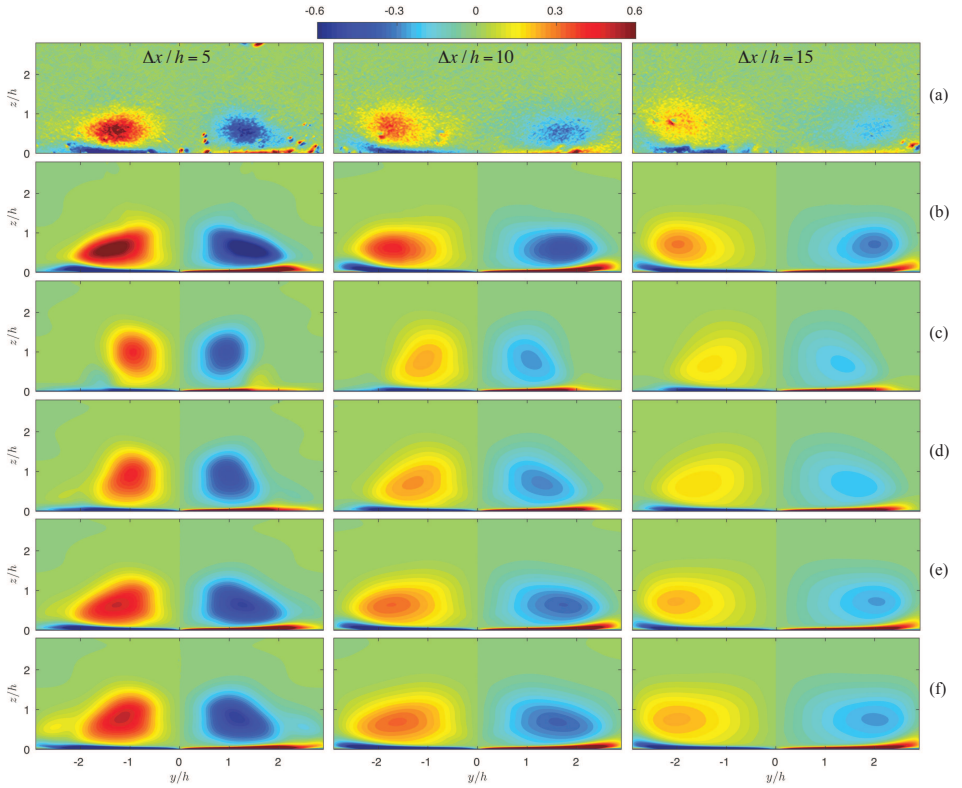

(b) Streamwise vorticity ($\omega_x \cdot h/U_\infty$)

Figure 12. Flow field snap shots for several simulation approaches for the flat plate case: (a) experimental data, (b) body fitted mesh, (c) BAY model, (d) uniform BAY model, (e) distributed $\mathbf{F}_{exact}$, (f) uniform $\mathbf{F}_{exact}$.

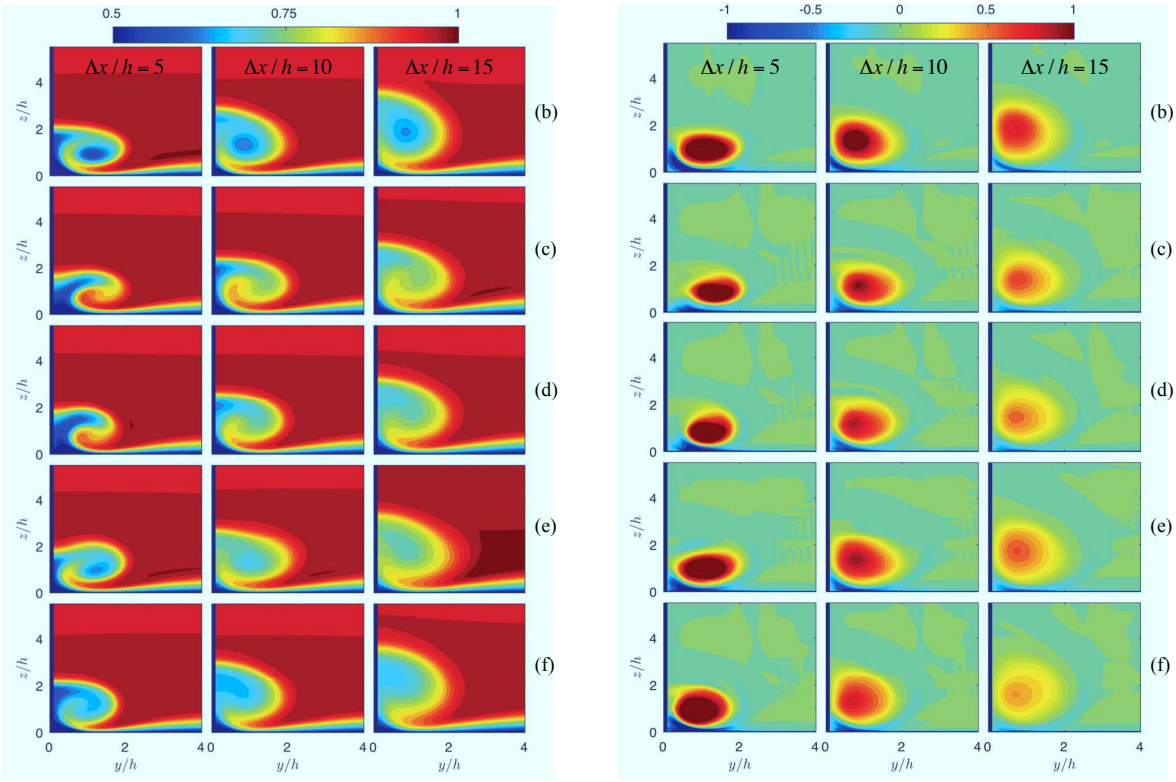

(a) Streamwise velocity (U_x/U_∞)

(b) Streamwise vorticity ($\omega_x \cdot h/U_\infty$)

Figure 13. Flow field snap shots for several simulation approaches for the airfoil case: (b) body fitted mesh, (c) BAY model, (d) uniform BAY model, (e) distributed $\mathbf{F}_{exact}$, (f) uniform $\mathbf{F}_{exact}$.

are expected to be significant for a possible improvement of the BAY model. Whereas previous efforts have focused on approaches to obtaining more realistic and smooth distributions of the source term over the selected cells,[18] our analysis indicates that a focus on the total force added by the source term could potentially be more effective in obtaining realistic flow fields. Especially improving the contribution in VG spanwise direction is expected to yield large improvements in the obtained flow field. Table 3 indicates that the underestimation of the force components of the BAY model is of the same order of magnitude in both considered cases. This could suggest that a simple, yet effective, empirical correction may be possible. However, additional research is required before being able to make conclusive statements in this respect.

VI. Conclusions

In this work the effectiveness of the BAY and jBAY models for including VG effects in CFD simulations is investigated. This is done by comparison with body fitted mesh simulations and by considering various mesh resolutions and alternative source term formulations.

It is observed that both the mesh resolution and the volume where the model is applied have a large impact on the flow field obtained with the BAY model. A more concentrated vortex is created upon refinement of the mesh. However, when approaching the body fitted mesh resolution the vortex intensity is still underestimated. Tuning the model by increasing the volume of application results in the creation of a stronger vortex and might be used to improve the circulation, but will not improve the overall accuracy of the flow representation. The jBAY model is able to partly avoid these problems, yielding a stronger vortex and reduced mesh dependence. However, for both models significant deviations in the boundary layer profile are observed on high resolution meshes. This suggests the presence of model errors which might result in poor predictions with respect to the VG effect on the flow.

Two factors defining the BAY model source term are investigated in more detail: the total resultant force added to the flow, and the distribution of the source term over the selected cells. Our analysis indicates

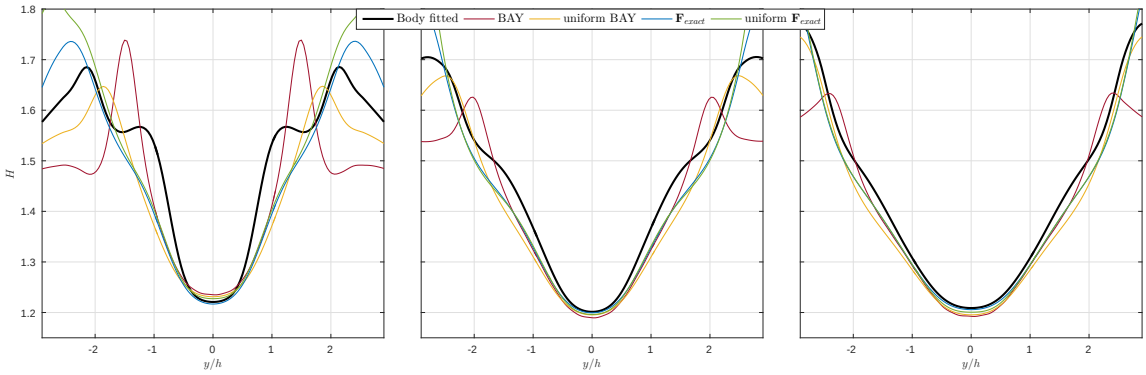

(a) Flat plate case.

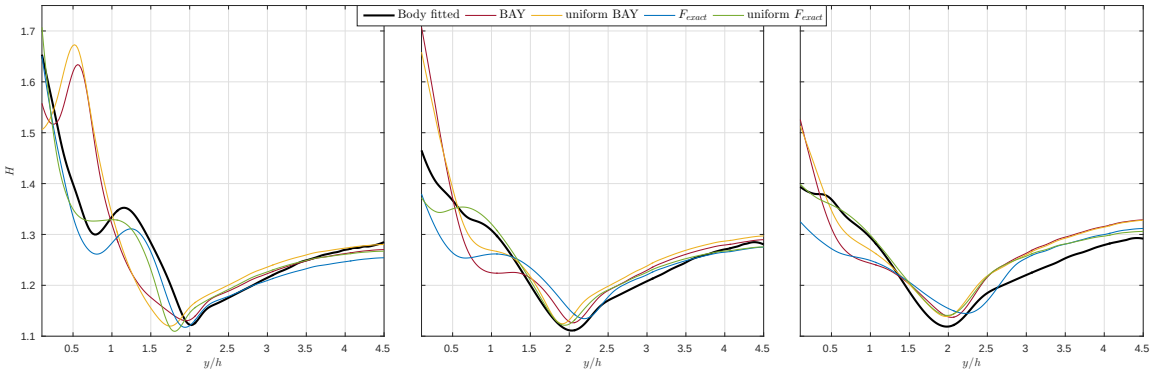

(b) Airfoil case.

Figure 14. Shape factor profiles for different simulation approaches at (from left to right) $\Delta x = 5h$, $\Delta x = 10h$ and $\Delta x = 15h$ behind the VG pair.

that the first one dominates both the strength and profile of the created streamwise vortex. Especially the component in the VG spanwise direction, despite being small in magnitude, has a significant effect on the shape of the created vortex. The large underestimation of this force component by the BAY model yields a poor prediction for the uplifting of fluid from the wall close behind the VG and therefore directly effects the flow profile. The distribution of the source term on the other hand seems to have minor influence on the characteristics of the created vortex.

Acknowledgments

This research is performed as part of the AVATAR project, which is funded by the FP7 programme of the European Union under grant agreement No FP7-ENERGY-2013-1/no.608396.

References

[1]Taylor, H., "The Elimination of Diffuser Separation by Vortex Generators," 1947.

[2]Gillen, T., Rybalko, M., and Loth, E., "Vortex Generators for Diffuser of Axisymmetric Supersonic Inlets," *5th Flow Control Conference*, American Institute of Aeronautics and Astronautics, Chicago, Illionois, jul 2010, pp. 1–18.

[3]Gyatt, G., "Development and testing of vortex generators for small horizontal axis wind turbines," *Renewable Energy*, 1986.

[4]Timmer, W. A. and van Rooij, R. P. J. O. M., "Roughness Sensitivity Considerations for Thick Rotor Blade Airfoils," *AIAA paper*, Vol. 125, No. 350, 2003, pp. 1–10.

[5]Tai, T. C., "Effect of Midwing Vortex Generators on V-22 Aircraft Forward-Flight Aerodynamics," *Journal of Aircraft*, Vol. 40, No. 4, 2003, pp. 623–630.

[6]Lin, J. C., "Review of research on low-profile vortex generators to control boundary-layer separation," *Progress in*

Aerospace Sciences, Vol. 38, No. 4-5, 2002, pp. 389–420.

[7]Kerho, M. and Kramer, B., "Enhanced Airfoil Design Incorporating Boundary-Layer Mixing Devices," *41st Aerospace Sciences Meeting and Exhibit*, American Institute of Aeronautics and Astronautics, Reston, Virigina, jan 2003.

[8]Skrzypiński, W., Gaunaa, M., and Bak, C., "The Effect of Mounting Vortex Generators on the DTU 10MW Reference Wind Turbine Blade," *Journal of Physics: Conference Series*, Vol. 524, jun 2014, pp. 012034.

[9]Ghosh, S., Choi, J.-I., and Edwards, J. R., "Numerical Simulations of Effects of Micro Vortex Generators Using Immersed-Boundary Methods," *AIAA Journal*, Vol. 48, No. 1, 2010, pp. 92–103.

[10]Shan, H., "Numerical simulation of flow behind active vortex generators with direct forcing immersed boundary method," *International Journal of Computational Fluid Dynamics*, Vol. 21, No. 1, 2007, pp. 49–60.

[11]Kunik, W. G., "Application of a computational model for vortex generators in subsonic internal flows," *AIAA/ASME/SAE/ASEE 22nd Joint Propulsion Conference*, 1986, pp. 0–6.

[12]Wendt, B. J., "Initial Circulation and Peak Vorticity Behavior of Vortices Shed from Airfoil Vortex Generators," Tech. Rep. August, NASA, 2001.

[13]May, N., "A new vortex generator model for use in complex configuration CFD solvers," *19th AIAA Applied Aerodynamics Conference*, American Institute of Aeronautics and Astronautics, Reston, Virigina, jun 2001.

[14]Törnblom, O. and Johansson, A. V., "A Reynolds stress closure description of separation control with vortex generators in a plane asymmetric diffuser," *Physics of Fluids*, Vol. 19, No. 11, 2007.

[15]Stillfried, F. V., Wallin, S., and Johansson, A. V., "Vortex-Generator Models for Zero- and Adverse-Pressure-Gradient Flows," *AIAA Journal*, Vol. 50, No. 4, 2012, pp. 855–866.

[16]Velte, C. M., "Vortex Generator Flow Model Based on Self-Similarity," *AIAA Journal*, Vol. 51, No. 2, feb 2013, pp. 526–529.

[17]Bender, E. E., Anderson, B. H., and Yagle, P. J., "Vortex Generator Modeling for Navier-Stokes Codes," *3rd Joint ASME/JSME Fluids Engineering Conference*, San Francisco, CA, 1999, pp. 1–7.

[18]Jirasek, A., "Vortex-Generator Model and Its Application to Flow Control," *Journal of Aircraft*, Vol. 42, No. 6, 2005, pp. 1486–1491.

[19]Wallin, F. and Eriksson, L.-E., "A Tuning-free Body-Force Vortex Generator Model," *44th AIAA Aerospace Sciences Meeting and Exhibit*, American Institute of Aeronautics and Astronautics, Reston, Virigina, jan 2006, pp. 1–12.

[20]Waithe, K., "Source Term Model for Vortex Generator Vanes in a Navier-Stokes Computer Code," *42nd AIAA Aerospace Sciences Meeting and Exhibit*, American Institute of Aeronautics and Astronautics, Reston, Virigina, jan 2004, pp. 1–11.

[21]Dudek, J. C., "Modeling Vortex Generators in a Navier-Stokes Code," *AIAA Journal*, Vol. 49, No. 4, 2011, pp. 748–759.

[22]Réthoré, P.-E., van der Laan, P., Troldborg, N., Zahle, F., and Sørensen, N. N., "Verification and validation of an actuator disc model," *Wind Energy*, Vol. 17, No. 6, jun 2014, pp. 919–937.

[23]Spalart, P. R., Shur, M. L., Strelets, M. K., and Travin, A. K., "Direct Simulation and RANS Modelling of a Vortex Generator Flow," *Flow, Turbulence and Combustion*, Vol. 95, No. 2-3, 2015, pp. 335–350.

[24]Menter, F. R., "Zonal Two Equation k-w Turbulence Models for Aerodynamic Flows," *24th Fluid Dynamics Conference*, Orlando, Florida, 1993.

[25]Baldacchino, D., Ragni, D., Simao Ferreira, C., and van Bussel, G., "Towards integral boundary layer modelling of vane-type vortex generators," *45th AIAA Fluid Dynamics Conference*, American Institute of Aeronautics and Astronautics, Reston, Virginia, jun 2015.

[26]Manolesos, M. and Voutsinas, S. G., "Experimental investigation of the flow past passive vortex generators on an airfoil experiencing three-dimensional separation," *Journal of Wind Engineering and Industrial Aerodynamics*, Vol. 142, 2015, pp. 130–148.

[27]Joubert, G., Le Pape, A., and Huberson, S., "Numerical study of flow separation control over a OA209 Airfoil using Deployable Vortex Generator," *49th AIAA Aerospace Sciences Meeting including the New Horizons Forum and Aerospace Exposition*, , No. January, 2011, pp. 1–20.

[28]Manolesos, M., Papadakis, G., and Voutsinas, S. G., "Assessment of the CFD capabilities to predict aerodynamic flows in presence of VG arrays," *Journal of Physics: Conference Series*, Vol. 524, jun 2014, pp. 012029.